

Intercalation and Staging Behavior in Super-Oxygenated $\text{La}_2\text{CuO}_{4+\delta}$

B.O. Wells¹, R.J. Birgeneau¹, F.C. Chou¹, Y. Endoh², D.C. Johnston³, M.A. Kastner¹, Y.S. Lee¹,
G. Shirane⁴, J.M. Tranquada⁴, and K. Yamada²

¹ Department of Physics and Center for Materials Science and Engineering, Massachusetts Institute of Technology, Cambridge, MA, 02139, USA

² Department of Physics, Tohoku University, Aramaki Aoba, Sendai, 980-77, Japan

³ Ames Laboratory and Department of Physics and Astronomy, Iowa State University, Ames, IA 50011, USA

⁴ Department of Physics, Brookhaven National Laboratory, Upton, NY 11973, USA

Abstract

A high temperature electrochemical oxidation process has been used to produce large single crystals of $\text{La}_2\text{CuO}_{4+\delta}$ suitable for neutron scattering experiments. Below room temperature the oxygen-rich phases have structural superlattice scattering peaks which indicate new periodicities ranging from 2 to 6.6 layers perpendicular to the copper oxide planes. A model structure originally proposed for $\text{La}_2\text{NiO}_{4+\delta}$ can account for the superlattice peaks as a result of anti-phase domain boundaries between different tilt directions of the CuO_6 octahedra. Within this model, the changes in CuO_6 tilt directions are induced by segregated layers of interstitial oxygen which order in a manner similar to intercalants in graphite. This structural model thus clarifies previous work and establishes $\text{La}_2\text{CuO}_{4+\delta}$ as a unique lamellar superconducting system with annealed disorder.

PACS Index Nos: 74.72.Dn, 74.25.Dw, 74.80.Dm, 61.12.-q

1 Introduction

One of the central questions concerning the physics of high temperature superconductors is how the physical properties evolve as a function of doping. The planar copper oxides are antiferromagnetic insulators when undoped. The addition of charge carriers makes them high temperature superconductors. For example $\text{La}_{2-x}\text{Sr}_x\text{CuO}_4$ is an insulating antiferromagnet for $x=0$ and a high temperature superconductor with a maximum T_c of about 38 K for $x=0.15$. An alternative method for doping $\text{La}_{2-x}\text{Sr}_x\text{CuO}_4$ is to add extra oxygen to form $\text{La}_2\text{CuO}_{4+\delta}$. Very high pressures are needed to oxidize La_2CuO_4 by annealing in oxygen at high temperatures, with pressures as high as 25 kbar needed to obtain single phase superconducting samples.[1] However, by using electrochemical techniques it is possible to prepare heavily oxygenated samples with δ as large as 0.12.[2, 3] $\text{La}_2\text{CuO}_{4+\delta}$ is superconducting for large values of δ with a maximum of T_c of 45 K.[4]

Much of the interest in $\text{La}_2\text{CuO}_{4+\delta}$ is focused on the observation of an intrinsic phase separation of the oxygen dopants. For oxygen contents such that $0.01 \leq \delta \leq 0.06$ and temperatures below 300 K, $\text{La}_2\text{CuO}_{4+\delta}$ spontaneously separates into metallic, oxygen-rich and insulating, oxygen-poor regions.[5, 6] This phase separation is not a well understood phenomenon. In particular, the structure of the oxygen-rich phase is not known. Undoped La_2CuO_4 has a fairly simple, body centered tetragonal structure at high temperatures. At 530 K there is a tetragonal to orthorhombic transition which is characterized by a tilting of the octahedra made up of the Cu atom and its six nearest neighbor oxygens around the tetragonal (1,1,0) axis.[7, 8] Most previous studies [9, 10] have reported that at low temperatures the oxygen-rich phase has, on average, a simple face centered orthorhombic structure, with no tilting of the CuO_6 octahedra. The occurrence of such a structure is surprising because it is not clear how the interstitial oxygen would suppress the tilting of the octahedra, or why the untilted structure would be orthorhombic. There have been reports of extra superlattice reflections in both neutron scattering [9] and electron diffraction [11] but these have not been understood in terms of the structure of $\text{La}_2\text{CuO}_{4+\delta}$.

In this paper we report a neutron scattering investigation of single crystals of $\text{La}_2\text{CuO}_{4+\delta}$. We have found that the low temperature structure of $\text{La}_2\text{CuO}_{4+\delta}$ is orthorhombic with a superlattice structure along the c axis. The diffraction is consistent with a structural model previously proposed for $\text{La}_2\text{NiO}_{4+\delta}$. [12] In this model the CuO_6 octahedra are tilted. Within the planes, the tilts are ordered in the same manner as in undoped La_2CuO_4 and perpendicular to the planes the tilts

have the same local ordering. The structure of $\text{La}_2\text{CuO}_{4+\delta}$ with $\delta \geq 0.06$ differs from that of La_2CuO_4 in that the doped material contains broad antiphase domain boundaries regularly spaced along the c axis, perpendicular to the CuO_2 planes. The antiphase domain boundaries consist of layers across which the direction of the CuO_6 tilts are reversed. Within this model the antiphase boundaries are presumed to be caused by ordered layers of interstitial oxygen. This one-dimensional ordering of the extra oxygen is similar to the staging behavior of halogens or alkalis intercalated into graphite.[13] Following the literature on intercalated graphite, we use the term staging to describe the c axis modulation of the undoped structure; stage n refers to an induced periodicity of n CuO_2 host layers. $\text{La}_2\text{CuO}_{4+\delta}$ thus presents an interesting contrast with $\text{La}_{2-x}\text{Sr}_x\text{CuO}_4$ since the dopants which contribute the charge carriers give rise to annealed rather than quenched disorder. This makes $\text{La}_2\text{CuO}_{4+\delta}$ a particularly rich system for studies of transport, magnetic, and superconducting properties.

This paper is organized into several sections as outlined below. Section 2 describes the sample preparation and measurement techniques. Section 3 presents our neutron measurements that determine the structure of the electrochemically oxygenated samples. In section 4 we summarize the model of Tranquada *et al.* [12] and show that it is consistent with the neutron data. Section 5 compares our results with previous experiments on $\text{La}_2\text{CuO}_{4+\delta}$. This compound is compared with $\text{La}_2\text{NiO}_{4+\delta}$ in section 6. In section 7 we present results on a crystal which clearly shows both staging and phase separation. Section 8 summarizes the primary results and conclusions of this work.

2 Experimental Procedures

Several single crystal samples with different oxygen contents were used in this experiment. Five different crystals were measured, one of which was studied at two different stages of oxidation. The three crystals, A, B, and D, were grown at MIT by the top seeded solution method.[14] Sample C was grown at AT&T Bell Laboratories by the flux method.[15] Sample E was grown at MIT using the travelling-solvent-floating-zone (TSFZ) technique. This latter method generally produces purer crystals since it does not involve the use of a crucible. All five crystals were electrochemically oxygenated. The electrolysis for sample C took place in a 1 N solution of NaOH in water. The

electrolysis current was fixed to values which restricted the voltage to less than 0.6 Volts with respect to a Ag/AgCl reference electrode in order to avoid the electrolysis of water. The oxidation took place at room temperature and continued for two months. Sample C was designated as “crystal B” in reference [16] and further details of the preparation and characterization of sample C are available there.[16] The electrolysis of samples A, B, D, and E was carried out in the same electrolyte but with a fixed voltage of 0.4V or 0.45V with respect to the Ag/AgCl reference electrode. In addition, the electrolysis was performed at elevated temperatures to speed the oxidation process. Samples A1 and A2 refer to the same crystal A after different amounts of electrolysis. Table 1 summarizes the material and electrolysis parameters of the six samples.

The samples have been characterized with bulk magnetization measurements in a Quantum Design SQUID magnetometer. Figure 1 shows magnetization measurements of sample B in a field of 0.5 T taken at weekly intervals during the oxidation process. The magnetization for the as-grown crystal has a peak at 225 K indicating the Néel temperature, T_N . The peak in the susceptibility is actually caused by the weak ferromagnetic transition which accompanies the antiferromagnetism.[17] At this point the sample shows no sign of superconductivity above 5 K. After one week, the peak in the magnetization is much broader and is shifted to a lower temperature. The center of this broad peak is near 150 K. In addition, low temperature, low field magnetization, not shown, shows a shielding signal with an onset near 29 K indicative of superconductivity, which is broad in temperature. This suggests that after a week of electrolysis, the crystal contains a distribution of oxygen contents and does not show two phase coexistence, presumably because of kinetic limitations. After another week of oxidation, the large Néel peak disappears and only a small residual Néel peak at 220 K remains. At this point the shielding measurement gives a large signal for superconductivity with a fairly broad transition and $T_c=29$ K at onset. (We note parenthetically here that superconducting T_c 's for crucible-grown single crystals are typically somewhat lower than those of nominally equivalent ceramics.) The crystal now exhibits the coexistence of two phases, an oxygen-poor phase with $T_N=220$ K and an oxygen-rich superconducting phase. The peak at T_N continues to shrink as the crystal is further oxidized. Most of the change in the macroscopic magnetization takes place in the first two weeks. After the completion of the electrolysis procedure, the remnant peak is approximately 1/15 of the original Néel peak, indicating the fraction of the sample that remains in the oxygen-poor phase.

Diffraction measurements were performed at beam lines H7 and H8 at the High Flux Beam Reactor at Brookhaven National Laboratory. The monochromators and analyzers were pyrolytic graphite (PG) set for the (002) reflection. Many different configurations were used in these experiments. Two PG filters were used to suppress reflections from $\lambda/2$ and $\lambda/3$ neutrons. Collimations used varied from $40' - 40' - S - 80' - 80'$ to measure weak superlattice peaks in small samples to $10' - 10' - S - 10' - 10'$ for high resolution measurements of fundamental peaks. All of the samples studied were wrapped with Al, sealed in an Al can with He exchange gas, and cooled in a Displex closed cycle He cryostat. Temperature was measured with a Pt resistance thermometer and a Si diode attached to the cold finger.

3 Structural Data

Figure 2 shows a real space model of $\text{La}_2\text{CuO}_{4+\delta}$. Part a is the orthorhombic Bmab structure of the undoped material and part b is the proposed modification of the structure for oxygenated $\text{La}_2\text{CuO}_{4+\delta}$, in analogy to the corresponding structure [12] in $\text{La}_2\text{NiO}_{4+\delta}$. This will be discussed in more detail below. A map of the attendant reciprocal space indexed to the orthorhombic Bmab unit cell is shown in Figure 2c. In this paper we use the notation \mathbf{a} , \mathbf{b} , \mathbf{c} to refer to the orthorhombic Bmab real space axes, and H, K, L for reciprocal space axes as well as general peaks at (H,K,L), with reciprocal lattice constants \mathbf{a}^* , \mathbf{b}^* , and \mathbf{c}^* . Neutron scattering measurements using a triple axis spectrometer are restricted to a plane in reciprocal space. Due to the \mathbf{a} - \mathbf{b} twinning present in La_2CuO_4 , our scattering plane is a superposition of the (H,0,L) and (0,K,L) planes. The fundamental or Fmmm peaks in this plane occur where both H and L are even or K and L are even. In addition, the Bmab phase has superlattice reflections which occur for H=0, K odd, and L even.

In Figure 3 we show the scattering profiles for samples C, A2, D and E along the L axis in the vicinity of the (0,1,4) position of reciprocal space. Each scan shows several peaks. In samples E, D, and A2, the (0,1,4) Bmab peak is visible. In addition, there are peaks at non-integer values of L. These peaks appear in pairs, in which each member is split from the (0,1,4) position by an amount Δ . Sample E has $\Delta = 0.15$, sample D has $\Delta = 0.18$, sample A2 has $\Delta = 0.25$, and sample C has $\Delta = 0.25, 0.33$, and 0.5 . Figure 2c indicates the positions of these peaks in reciprocal space for $\Delta = 0.25$. With $\Delta = 1/n$, the superstructure peaks at larger Δ are at integer values of n

whereas those at smaller Δ are incommensurate; for sample E, $n=6.6$, for sample D, $n=5.5$, for sample A2, $n=4$, and for sample C, $n=2, 3$ and 4 . Sample A1 also has $n=5.5$ and sample B has $n=4.2$. The four samples in Figure 3 illustrate the range of values we have detected for Δ , or n .

Figure 4 shows the diffraction profile along L for sample B, a sample with close to the stage 4 structure, in the vicinity of the $(0,3,2)$ Bmab superlattice peak. The data in this figure cover a wider range in L than shown in Figure 3. Well-developed peaks are seen near $(0,3,2 \pm \frac{1}{4})$, but any peaks at the positions of the higher harmonics of $(0,3,2 \pm \frac{3}{4})$ are hardly detectable. There does appear to be a very small peak at $(0,3,1\frac{1}{4})$ which is about 1/100 of the intensity of the $(0,3,1\frac{3}{4})$ peak. This is the only higher harmonic peak that we have found throughout the $(H,0,L)/(0,K,L)$ zone. We also have conducted an extensive search for other superlattice peaks. In particular, we have searched for peaks that would correspond to a new in-plane ordering including scans in H or K with L an integer or at a staging position ($L = \text{integer} \pm 1/n$) as well as scans in L at various values of H or K. We have found no other superlattice peaks within the $(H,0,L)/(0,K,L)$ zones.

A practical way to distinguish scattering peaks from the oxygen-rich and oxygen-poor phases is through the differing length of the c axis lattice constant. A high resolution scan of the fundamental $(0,0,8)$ position shows two peaks indicating that there are two phases with different lattice parameters present in the sample. The values for the c lattice constants are shown in Figure 5a. One peak corresponds to the position of the $(0,1,4)$ Bmab superlattice peak while the other corresponds to the average of the $(0,1,4 \pm \Delta)$ peaks. Thus the peaks at $(0,1,4)$ and $(0,1,4 \pm \Delta)$ are from separate phases. From the intensity of the two $(0,0,8)$ peaks, we can estimate the fraction of the sample in the Bmab and staged phases. For example, in sample B the ratio of $(0,0,8)$ peak intensities indicates that about 5% of the sample is oxygen-poor. This compares well with the relative strength of the Néel peak in the magnetization curve of Figure 1 which indicates that 7% of the sample is oxygen-poor. For the samples in Figure 3, we find that sample E is 80% oxygen-poor, sample D is 27% oxygen-poor, and sample A2 is 2% oxygen-poor. The Bmab peaks in samples D and A2 look large in comparison to the staging peaks because they are much narrower. A high resolution scan of the $(0,0,8)$ peak in sample C indicates that several phases are present, but even the highest spectrometer resolution is inadequate to distinguish them.

Figure 5 shows the lattice constants we measure for samples A1, B and C. For samples A1 and B lattice parameters for both the minority oxygen-poor and the majority oxygen-rich phase

are given. For sample C, we are not able to resolve peaks from the different phases, so the given values are an average of the three staged phases that are present. There is a large expansion of the **c** axis for the staged samples compared to the undoped phases. We expect such an increase in volume to accommodate the doped interstitial oxygens. However, there is only a slight increase in the **c** axis between the stage 5.5 phase and the stage 4 phase and no further expansion for the stage 2-4 sample. Comparing the **a** and **b** axes for the different phases shows that the introduction of extra oxygen causes a contraction of the in-plane lattice constants, although, once again, the differences in the in-plane lattice constants between the oxygen-poor phase and the oxygen-rich phase is much greater than the differences between differently staged phases. The behavior of the lattice constants in $\text{La}_{2-x}\text{Sr}_x\text{CuO}_4$ is very similar. For Sr contents less than $x \sim 0.01$, the **a**-axis shrinks and the **c**-axis grows with increasing x , while for Sr contents greater than $x \sim 0.01$, that is, Sr contents corresponding to superconducting phases, the $\frac{\mathbf{a}+\mathbf{b}}{2}$ and **c** lattice constants are nearly independent of x . [18] As discussed below, the lowest density oxygen-rich phase we observe corresponds to $\delta \sim 0.06$ or a hole concentration equivalent to $\text{La}_{2-x}\text{Sr}_x\text{CuO}_4$ with x as high as 0.12. The exact hole concentration (p) as a function of δ in $\text{La}_2\text{CuO}_{4+\delta}$ samples depends on the ionization state of the intercalated oxygens and this is a matter of debate in the literature with reported values of p/δ ranging from 1 to 2. [4, 9, 19, 20]

The orthorhombic phase is stable to higher temperatures for the phases with lower staging numbers. Undoped La_2CuO_4 has a transition from a high temperature tetragonal phase (HTT) to a low temperature orthorhombic phase (LTO) at approximately 530 K. While we did not raise the temperature high enough to observe the transition in the oxygen-rich phases, the stage 5.5 sample has the smallest orthorhombic strain at room temperature and should become tetragonal at the lowest temperature. Extrapolating from the data in Figure 5 indicates that the HTT to LTO transition is near 400 K in the stage 5.5 sample. As the stage number decreases, the orthorhombic strain increases, and presumably, the phase transition to the tetragonal phase moves to higher temperatures. Thus, initially the tetragonal to orthorhombic transition temperature decreases with the introduction of extra oxygen, but then rises as the staging number is lowered. This same behavior of the HTT to LTO transition has also been reported by Radaelli *et al.*. [6] In $\text{La}_{2-x}\text{Sr}_x\text{CuO}_4$ on the other hand, the temperature of the tetragonal to orthorhombic phase transition decreases monotonically with increasing Sr content, and the material remain tetragonal at the lowest temperatures

measured for a Sr content of 0.2 or more.[8]

The temperature dependence of the staging peaks indicates that the various stagings are equilibrium phases. Three different samples include stage 4 phases: samples A2 and B are greater than 90% stage 4 while sample C has a minority stage 4 phase. Figure 6 shows the temperature behavior of the $(0,3,2 \pm \frac{1}{4})$ peak for the stage 4 phases in samples B and C. The integrated intensity and the in- and out-of-plane half-widths-at-half-maxima (HWHM) are shown. These data are derived from fits of the in- and out-of-plane directions of the stage 4 peak in sample B. In the simplest model the widths of these peaks are proportional to the inverse of the size of the coherent patches of stage 4 phase. Sample B has ordered domains that are 120Å wide in-plane and 60Å out-of-plane while the domains in sample C are 230Å in-plane and 130Å out-of-plane. Here we have taken the domain size as the inverse of the de-convolved HWHM. It should be noted that the out-of-plane widths may also arise in part from staging disorder, with the stage 4 peak representative of a mixture of stages 3, 4 and 5. Staging disorder is likely to be a major contributor to the peak broadening for the stage 5.5 and 6.6 phases which more clearly represent mixtures of pure stages. The difference in domain size may reflect the quality of the initial La_2CuO_4 crystal, or alternatively, may indicate the equilibrium domain size. The integrated intensity in the two crystals falls off in the same manner with increasing temperature indicating an ordering temperature of about 300 K. As noted before, the stage 5.5 peak has a similar temperature dependence to that of the stage 4 peak, ordering near 300 K. The stage 2 and 3 peaks remain ordered to higher temperatures. We have observed very little dependence of the widths or intensities of these staging peaks on the rate at which the sample is cooled, indicating that the time scale for ordering the staging domains is smaller than the time over which we can cool the sample. The cooling rate for the displex cryostats used in the neutron scattering experiments is fairly slow, taking about 3 hours to cool to 10 K from room temperature. As we point out below, in susceptibility measurements, for which we can quench more quickly, the crystals show indications of an ordering time of at least several seconds.

4 The Structural Model

In order to explain the diffraction peaks we use a structural model previously presented for $\text{La}_2\text{NiO}_{4+\delta}$ by Tranquada *et al.*[12] To explain the model, we use several simplifications. We

refer to CuO_6 octahedra when, in fact, even in the undoped material the CuO_6 complex does not form a perfect octahedron.[7, 8] Furthermore, the true distortions involved in the tetragonal to orthorhombic transition are more complicated than simple rotations of the CuO_6 complex. However, the symmetries produced by the structural distortions are the same as those that would be produced by a rigid rotation of the CuO_6 unit, and this description provides an easily understood description of the various structures involved in this study. In addition, we describe the model as having absolutely sharp domain boundaries and completely segregated sheets of oxygen. In fact, it is likely that the domain walls and oxygen sheets are spread across a few atomic layers. In some cases, we have strong evidence for such smearing of the boundaries, as we point out below.

At high temperatures undoped La_2CuO_4 has the body centered, tetragonal K_2NiF_4 structure, with space group Immm , the HTT phase.[8] This structure consists of sheets of CuO_6 octahedra sharing in-plane corners. La ions are nearly coplanar with the apical oxygen ions. At 530 K there is a phase transition to an orthorhombic structure with space group Bmab , the LTO phase. This orthorhombic structure is achieved by tilting the octahedra along a direction at 45° with respect to the Cu-O in-plane bonds, that is, around the orthorhombic [100] direction. Because each in-plane O ion is shared between two CuO_6 octahedra, adjacent oxygen-sharing octahedra must tilt in opposite directions as illustrated in Figure 2. The apical oxygens are not shared between CuO_6 octahedra in different layers so only weaker electrostatic forces determine the alignment of tilts from layer to layer. In the Bmab structure the alignment of adjacent planes is such that all octahedra with the same displacement along b tilt in the same direction. This is illustrated in Figure 2a.

As noted above, the reciprocal space cell that we are using is referred to a unit cell for the orthorhombic, Bmab structure. This orthorhombic unit cell has twice the in-plane area of the primitive unit cell for the HTT structure. The scattering for the tetragonal phase in the zone accessible in this experiment gives Bragg peaks at $(H \text{ even}, K=0, L \text{ even})$. A simple orthorhombic distortion, in which the only change is a stretching of the \mathbf{b} axis, leads to what is known as the Fmmm structure. This structure gives the same scattering as observed in the tetragonal case except that $H \neq K$, and because of twinning, both zones $(H,0,L)$ and $(0,K,L)$ are observed in our scattering geometry. The Bmab superstructure, which is generated by the displacements attendant with the octahedra tilts, gives rise to superlattice peaks in the neutron scattering in the $(H,0,L)/(0,K,L)$

zone at positions ($H=0$, K odd, L even). The oxygenated crystals show a splitting of the Bmab superlattice peaks along L , but we have failed to observe new peaks at values of $H \neq 0$. Qualitatively, the scattering pattern reveals the following about the structure of $\text{La}_2\text{CuO}_{4+\delta}$:

1. a new periodicity along \mathbf{c} , n times the original \mathbf{c} lattice constant,
2. the change involves the octahedra tilts, and
3. there are no displacements along the $[1,0,0]$ direction that lead to new symmetries.

These points are included in the model structure for $\text{La}_2\text{CuO}_{4+\delta}$ that we discuss below.

The underlying physics of this model is as follows. It has been suggested by Chaillout *et al.* [21] that the interstitial oxygen atoms sit in the $(1/4, 1/4, 1/4)$ sites of the orthorhombic unit cell. This site is between pairs of layers containing La and apical O atoms, directly above an in-plane oxygen. A single negatively charged oxygen ion in such a site repels nearest neighbor apical oxygen ions and attracts La ions. A local tilt flip of the CuO_6 octahedron either above or below the excess oxygen ion creates a large interstitial position and maximizes the average distance between the extra oxygen ion and surrounding oxygen ions. Within a layer, the flipped tilt pattern propagates because of the shared corner oxygens. In turn, this creates an entire array of favorable interstitial sites in the same plane as the original interstitial oxygen. We illustrate such an arrangement in Figure 2b. Other interstitials fill this plane, but electrostatic repulsion between oxygen ions or the number of available sites limits the density within any one interstitial layer. The spacing between interstitial layers is governed by long range strain energies.[13] Between planes of interstitial oxygen ions, the structure is still Bmab, but in addition, anti-phase boundaries between the two possible Bmab orientations exist at every layer of interstitial oxygen ions.

We have calculated the structure factors for the model proposed above in order to compare the scattering it predicts with experiment. The calculations have been performed for a single, expanded unit cell that represents the full symmetry of a perfectly staged sample. For example, for a stage 4 phase, our unit cell is the same as for the orthorhombic Bmab phase in the \mathbf{a} and \mathbf{b} directions, but it is 4 Bmab unit cells long in the \mathbf{c} direction. This large unit cell contains 8 CuO_2 layers, the first four with octahedral tilts in one direction and the next four with the opposite tilt direction. The effect of this variation on the Bmab structure is that the Bmab superlattice peaks at $(0, K \text{ odd}, L \text{ even})$ have zero amplitude in the structure factor and are replaced by peaks displaced

along the L axis by $\pm 0.25\mathbf{c}^*$ and $\pm 0.75\mathbf{c}^*$. The positions of the allowed peaks and the general intensity variation of our calculated structure factors throughout reciprocal space are in agreement with the data. However, the octahedra must be distorted to match quantitatively the intensities of the peaks throughout the zone. Determining this distortion unambiguously is impossible with the few superlattice peaks we have measured. For our calculation, we have used the atomic positions given by Zolliker *et al.* [22] for the LTO, undoped phase. These correspond to CuO_2 octahedral tilts of 5.5 degrees.

The structure factor calculation for this model predicts peaks at positions that correspond to higher odd harmonics of the staging peaks. That is, for the stage 4 sample, the calculation gives first harmonic peaks at $(0, K \text{ odd}, L = \text{even} \pm 1/n)$ and third harmonic peaks at $(0, K \text{ odd}, L = \text{even} \pm 3/n)$. The third harmonic peaks are predicted to be weak, but definitely stronger than any seen in the data. For example, the calculation predicts that the strongest third harmonic peak, over the range of reciprocal space that we have studied, is the $(0, 3, 1\frac{1}{4})$ peak which is 1/5 the calculated intensity of the $(0, 3, 1\frac{3}{4})$ peak. As shown in Figure 4 however, the $(0, 3, 1\frac{1}{4})$ peak is only about 1/100 the intensity of the $(0, 3, 1\frac{3}{4})$ peak. We can account for this suppression of the higher harmonic peaks by allowing a variation in the degree of tilt of the CuO_6 octahedra. The original model allows only for a tilt of $+\Theta$ for the n layers on one side of the antiphase domain boundary and $-\Theta$ on the other. Thus for a given \mathbf{b} coordinate, the CuO_6 tilt angle forms a square wave along the \mathbf{c} direction. If the CuO_6 tilt angle forms a sine wave instead, then the scattering at higher harmonics of the staging periodicity is suppressed. For a stage 4 structure such a sine wave means that with each stack of four La_2CuO_4 layers, the two layers of CuO_6 octahedra bordering the domain boundaries have a smaller tilt angle than the octahedra in the two layers not adjacent to the boundary. The structure factor for this configuration with tilts of 5.5° and 2.75° for the inner and border CuO_6 octahedra respectively, predicts that the intensity of the $(0, 3, 1\frac{1}{4})$ peak is 1/100 of the intensity of the $(0, 3, 1\frac{3}{4})$ peak, in agreement with the data.

While the peaks displaced along L from the Bmab positions can be explained merely by the changing tilt directions of the CuO_6 octahedra, the intercalated layers of oxygen should themselves produce scattering peaks at $(0, 0, 2z/n)$, with n the staging number and z an integer. We do not observe such peaks above the background for samples A and B. In sample C, we do see peaks at $(0, 0, z)$ with z odd. This would correspond to peaks from the excess oxygen in stage 2. However,

our structure factor calculation shows the observed peaks are stronger than expected for scattering from the excess oxygen and may correspond to other effects such as expansion of the layer in which the excess oxygen is inserted. There are no detectable peaks at the positions for scattering from the intercalated oxygen for the stage 3, 4 or 5.5 phases. Thus, we have not been able to detect a scattering peak directly from the excess oxygen. We have performed structure factor calculations for our model structure in order to determine whether the peak for scattering directly from the interstitial oxygen ought to be strong enough to detect. Assuming an oxygen content of 4.0625 for a stage 4 sample, corresponding to 1/4 of the large interstitial sites occupied, and that all of the excess oxygen atoms are confined to the antiphase domain boundary layer, the $(0,0,2z/n)$ peaks should be approximately 1/100 of the $(0,3,1\frac{3}{4})$ peak shown in Figure 4. Such peaks should be just barely observable; the absence of these planar oxygen diffraction peaks argues for either staging disorder or a broader distribution of the intercalated oxygen.

5 Comparison to Other Results

Several other groups have proposed models for the structure of the oxygen-rich phases of $\text{La}_2\text{CuO}_{4+\delta}$. The model we have used is different from any used before for $\text{La}_2\text{CuO}_{4+\delta}$, but much of the actual data presented in the previous papers are consistent with both our data and the staging model. Our neutron scattering experiments provide a direct measure of the structure. We have used crystals with as great a range of oxygen contents as any previously studied, and our large crystals allow a higher resolution study than earlier experiments. This has allowed us to identify the weak, but essential, superlattice peaks which were missed or misidentified in earlier work.

A detailed comparison of our results with previous papers indicates that much of the earlier data are consistent with the oxygen-rich phases being staged. In particular, those papers which report that the oxygen-rich structure is Fmmm most likely simply missed the weak, broad staging superlattice peaks.[9, 10] These peaks would be particularly difficult to observe in powder samples. We do find that the Bmab superlattice peaks disappear in the oxygen-rich phase in agreement with Radaelli *et al.*[9] The staged peaks that replace the Bmab diffraction peaks can vary in width and intensity depending upon the overall oxygen content and the degree to which the staged tilt pattern is able to order. Vaknin *et al.* [10] report a broadening and weakening of the Bmab superlattice

peak at 260 K. They themselves note that this may be due to an unresolved splitting of the Bmab peak. Radaelli *et al.* [9] report neutron scattering measurements on a small single crystal doped beyond the phase separation region. The small size of their crystal limits the resolution that they are able to use and complicates the comparison to our data. They report several different sets of superlattice peaks. At least one set appears to be consistent with a stage 3 model. We do not detect any sign of the other superlattice peaks they report.

Above room temperature the staging peaks for the stage 4 and higher staged phases disappear. No other superlattice peaks appear at this temperature. Thus, above room temperature the average structure is Fmmm. In this case, the tilts presumably still exist, but are disordered. Indeed, this staging order-disorder transition warrants further study. If the tilt angle has a sine-wave distribution, the transition occurs at the temperature at which the amplitude of the sine-wave goes to zero. It is possible that in some of the previous experiments this Fmmm structure was locked in at lower temperatures by quenching the sample; this could also occur if a large number of defects pin the direction of the CuO_6 tilts and do not allow them to order. A separate, early neutron scattering experiment by Chaillout *et al.* [23] claims that the oxygen-rich phase is a distinct structure with the same Bmab symmetry as the oxygen-poor and undoped phase. Neither this experiment nor those listed above which claim that the oxygen-rich phase is Fmmm see diffraction peaks that could be consistent with such a structure.

Hammel *et al.* [24] use results from NMR and NQR experiments to propose a model in which the magnitude of the CuO_6 octahedral tilts vary within a plane. In this model there is a continuous variation of the tilt angle of neighboring CuO_6 octahedra displaced along the b axis from a maximum value of $+\Theta_{max}$ to a minimum of $-\Theta_{max}$. After reaching the value $-\Theta_{max}$, the next octahedron flips to $+\Theta_{max}$ and a favorable interstitial site is formed. This arrangement of CuO_6 tilts is not compatible with our structural diffraction data. We see no evidence for in-plane scattering peaks that would arise if such an arrangement of the CuO_6 octahedral tilts were ordered. However, our data do indicate that there is some distribution of tilt angles. As described above, in the stage 4 sample with a sine wave distribution of tilts, two different CuO_6 species are present, a small tilt in layers adjacent to the antiphase domain boundary and a larger tilt in those layers further from the boundary. Our neutron diffraction experiments only determine the average structure. If the values for the tilt angles were, for example, $2\frac{3}{4}$ and $5\frac{1}{2}$ degrees, with a variation

of plus or minus one degree for either, then there would be a fairly uniform distribution of local CuO_6 octahedral tilts, consistent with the NMR-NQR data.

The optical properties of our sample C have been measured by Quijada *et al.*[20] They have found that the 500 cm^{-1} mode of the apical oxygen atoms splits into two distinct components in the oxygen rich phase. It is difficult to make a direct comparison of this near surface measurement to our bulk structure determination for such a multi-phase sample. However, we speculate that the two components of the apical oxygen mode correspond to those apical oxygen atoms adjacent to the intercalated oxygen layers and those not neighboring the excess oxygen layers.

6 Comparison to $\text{La}_2\text{NiO}_{4+\delta}$

$\text{La}_2\text{NiO}_{4+\delta}$ exhibits many different structural phases as a function of the oxygen content as has been reported by Tranquada *et al.*[12] For oxygen contents $0.058 < \delta < 0.125$, $\text{La}_2\text{NiO}_{4+\delta}$ has staged phases with scattering profiles very similar to those we measure for $\text{La}_2\text{CuO}_{4+\delta}$. Both $\text{La}_2\text{NiO}_{4+\delta}$ and $\text{La}_2\text{CuO}_{4+\delta}$ are tetragonal at high temperatures. In $\text{La}_2\text{NiO}_{4+\delta}$ the staging peaks appear at the HTT to LTO phase transition at $T \leq 290\text{ K}$. In $\text{La}_2\text{CuO}_{4+\delta}$ for stage 4 and higher, the staging peaks order near room temperature, but this is well below the tetragonal to orthorhombic structural phase transition temperature. We have not determined whether the stage 2 and 3 phases order independently of the HTT to LTO structural transition.

Several different staged phases have been reported in various samples of $\text{La}_2\text{NiO}_{4+\delta}$. Slowly cooled, staged samples include the following:

1. a single superlattice indicating nearly pure stage 2 for $\delta=0.105$,
2. two superlattices indicating nearly pure stage 2 and stage 3 phases for $\delta=0.085$,
3. two superlattices indicating one phase with mixed stage 3 and 4 and a lightly oxygenated phase with the low temperature tetragonal structure (LTT) for $\delta=0.06$.

In all of these samples, broad scattering peaks that correspond to intermediate staging appear if the samples are cooled quickly. We have not seen such a dependence on cooling rate for $\text{La}_2\text{CuO}_{4+\delta}$. The time scale for ordering into staged structures appears to be less than one hour in $\text{La}_2\text{CuO}_{4+\delta}$, but is several hours in $\text{La}_2\text{NiO}_{4+\delta}$. [25] In addition, we detect a wider range of stagings than has

been seen in the nickel oxide materials. In $\text{La}_2\text{CuO}_{4+\delta}$ we have seen a range of stages from 2 to 6.6 while in $\text{La}_2\text{NiO}_{4+\delta}$, only stagings from 2 to 3.5 have been detected.

Most of the crystals of $\text{La}_2\text{CuO}_{4+\delta}$ and $\text{La}_2\text{NiO}_{4+\delta}$ studied show coexistence of phases of different pure integer stagings or a staged phase plus an oxygen-poor phase. Single superlattice peaks that represent mixed stage phases occur mostly for the larger staging numbers observed in either compound. The free energy difference between phases with large staging numbers must be very small so it may be particularly difficult to reach an equilibrium state for such configurations.

7 Phase Separation

Further experiments are necessary before we can reach strong conclusions about the relationship between staging and the separation of oxygen-rich and oxygen-poor phases. In this section we point out the implications of the work carried out so far. In only one of the samples studied to-date, sample E, have we been able to detect definite evidence of an equilibrium, temperature driven phase separation. The magnetization at high field revealing the weak ferromagnetic transition [17] associated with the antiferromagnetism of the undoped phase is shown in the top panel of Figure 7. The shielding signal for superconductivity in the oxygen-rich phase is shown in the lower panel. The temperature dependence of the high field magnetization is very similar for the pre- and post-electrolysis samples. Assuming that the per site magnitude of the weak ferromagnetic moment is similar as well, the weak ferromagnetic signal strength at low temperatures provides a measure of the volume of the sample that is oxygen-poor. Using this criterion, we find that below the phase separation temperature, sample E is 20% oxygen-rich and 80% oxygen-poor. We also see from the shielding measurement that the superconducting transition temperature is dependent on the cooling rate of the crystal. Slow cooling measurements are made after cooling the sample from room temperature to 50 K over approximately six hours. Alternatively, quenching the sample is accomplished by plunging it directly into the magnetometer which is already cooled to 5 K. Using this method the sample is cooled from room temperature to 10 K within 10 seconds. Slow cooling leads to a T_c of 32 K versus 26 K for the sample quenched from room temperature. However, there is a substantially larger shielding signal for the quenched sample. The difference in volume fraction of the shielding signal indicates that quenching lowers T_c by inhibiting the phase separation process.

A thorough discussion of the effects on T_c of quenching $\text{La}_2\text{CuO}_{4+\delta}$ is available elsewhere.[26] The much slower cooling rates available for the neutron scattering experiments do not allow us to study directly the effects of quenching on the structure. It should be noted that the T_c of sample E is higher than that of the others and the transition is sharper; we believe that this occurs because the parent La_2CuO_4 crystal is grown using the float zone technique and hence is purer than the crucible-grown crystals.

The relative intensities of the two (0,0,8) peaks provide a second measure of the fraction of the sample in the two phases. There may be some error in this calculation because there can be small variations in the structure factor for the (0,0,8) peak in the two phases. A fit of the (0,0,8) peak at low temperatures to two gaussians indicates that 16% of sample E is oxygen-rich and 84% is oxygen-poor. This result is comparable to that obtained from the relative strength of the weak ferromagnetic signals described above, which gave phase fractions of 20% and 80%, respectively. From the phase diagram previously determined by Radaelli *et al.* [6] for powder $\text{La}_2\text{CuO}_{4+\delta}$ samples we infer a macroscopic oxygen concentration of 4.02 for this sample with 80% $\delta=0.012$ and 20% $\delta=0.055$.

All of the samples we have studied show multiple phases. Five samples show coexistence of an oxygen-poor Bmab phase and a staged phase. Of these, A1, A2, B and D contain two phases at all temperatures studied. The highest measurement temperatures vary: sample A1 (stage 5.5), A2 (stage 4), and C (stages 2,3,4) have been measured up to 300 K, sample B (stage 4.2) has been measured up to 320 K, and sample D (stage 5.5) has been studied up to 390 K. There are two possible reasons why the latter four samples do not form a uniform phase. The first is that the phase separation temperature for these samples is simply higher than the temperatures at which they have been measured. The second is that the two phases result from macroscopically inhomogenous regions in the crystals rather than an equilibrium phase separation.

The phase diagrams that have been published by Radaelli *et al.* [6] and Hammel *et al.* [24] both show that the phase separation temperature for a sample near the oxygen-rich side of the miscibility gap is near 280 K. Because of this, we believe that the mostly stage 4 samples, A2 and B do not show true equilibrium phase separation. Rather, some small region of each sample is not in equilibrium with the majority of the crystal and remains oxygen-poor. It is more likely that samples A1 and D do show orthodox equilibrium phase separation since they both have substantial

oxygen-poor volume fractions. The phase separation temperature may be much higher in these samples. The phase diagrams determined by Radaelli *et al.* [6] and Hammel *et al.* [24] both indicate phase separation temperatures near 400 K for oxygen concentrations at the middle of the miscibility gap. We know that the stage 6.6 phase represents the structure of $\text{La}_2\text{CuO}_{4+\delta}$ at the lowest temperature, oxygen-rich edge of the miscibility gap in crystal E which was grown by the TSFZ method. We suspect that the phase at the oxygen rich side of the miscibility gap for crystals grown by the top-seeded solution method, as seen in samples A and D, is stage 5.5 The staging of the phase on the oxygen-rich side of the miscibility gap thus varies from crystal to crystal, probably because of the specific defects present in each crystal.

8 Summary and Conclusions

We have used a high temperature electrochemical process to produce large single crystals of super-oxygenated $\text{La}_2\text{CuO}_{4+\delta}$. Neutron scattering studies of these crystals reveal that the oxygen-rich phases in these crystals have a superstructure different from that observed in undoped or Sr-doped La_2CuO_4 . In particular, instead of superlattice peaks at Bmab symmetry positions, we find pairs of peaks that are displaced by equal amounts $\pm\Delta$ from the Bmab positions. We have proposed a model that attributes these peaks to a staging phenomenon, that is, the excess oxygen ions are ordered into regularly spaced interstitial planes. The ordering of the oxygens causes a series of anti-phase domain boundaries between tilt directions of the CuO_6 octahedra. A great deal of work remains to be done to understand completely the $\text{La}_2\text{CuO}_{4+\delta}$ staging phase diagram. The microscopic structure that we have measured for the oxygen-rich phases of $\text{La}_2\text{CuO}_{4+\delta}$, is quite different from what has been previously assumed. It is now necessary to revisit models for hole driven phase separation in light of our new understanding of the structures present on both sides of the miscibility gap.

An interesting and important difference between the $\text{La}_2\text{CuO}_{4+\delta}$ and $\text{La}_{2-x}\text{Sr}_x\text{CuO}_4$ superconducting systems is that in the former, the oxygen dopants give rise to annealed disorder whereas in the latter, the Sr dopants produce quenched disorder. By annealed disorder one means that in $\text{La}_2\text{CuO}_{4+\delta}$ the intercalated oxygen ions reach their equilibrium configuration at a temperature which, in energy units, is much less than the characteristic electronic and magnetic energies in this

system. By contrast in $\text{La}_{2-x}\text{Sr}_x\text{CuO}_4$ the Sr distribution is determined at the growth temperature and there is no further equilibration with respect to the Cu^{2+} magnetic or electronic system at lower temperatures. This is described as quenched disorder. Of course, it seems likely that in neither case is there equilibration with respect to the superconductivity. It will be very valuable to explore any possible differences in these two systems which reflect the differences in the nature of the dopant disorder.

Clearly studies of the transport, optical and microscopic magnetic properties of these novel $\text{La}_2\text{CuO}_{4+\delta}$ lamellar superconductors as a function of stage number would be most interesting. Many materials physics challenges remain as well. For example, it is essential to characterize quantitatively the relationship between the excess oxygen concentration and the stage number. On the materials preparation side we need to learn how to prepare larger single crystals with increased homogeneity, large and uniform staging domains, and sharp superconducting transitions.

The work at MIT was supported by the MRSEC Program of the National Science Foundation under award number DMR 94-00334 and by the NSF under award number DMR 93-15715. Research at Brookhaven National Laboratory was carried out under contract No. DE-AC-2-76CH00016, Division of Material Science, U.S. Department of Energy. Ames Laboratory is operated for the U.S. Department of Energy by Iowa State University under contract No. W-7405-Eng-82. The work at Ames was supported by the Director for Energy Research, Office of Basic Energy Sciences.

References

- [1] Zhou, J., Sinha, S., and Goodenough, J.B., Phys Rev.B **39**, 12331 (1989).
- [2] Wattiaux, A., Park, J., Grenier, J., and Bouchard, M., C.R. Acad. Sci.,Paris 310, Serie II, 1047 (1990).
- [3] Chou, F.C., Cho, J.H., and Johnston, D.C., Physica C**202**, 209 (1992).
- [4] For a review see Johnston, D.C., Borsa, F., Canfield, P.C., Cho, J.H., Chou, F.C., Miller, L.L., Torgeson, D.R., Vaknin, D., Zaretsky, J., Ziolo, J., Jorgensen, J.D., Radaelli, P.G., Shultz, A.J., Wagner, J.L., Cheong, S.-W., Bayless, W.R., Schirber, J.E., and Fisk, Z., in *Phase Separation in Cuprate Superconductors* ed. Sigmund, E., and Müller, K.A. (Springer-Verlag, Heidelberg, 1994) pp. 82-100.
- [5] Jorgensen, J.D., Dabrowski, B., Pei, S., Hink, D.G., Soderholm, L., Morosin, B. Schirber, J.E., Venturini, E.L., and Ginley, D.S., Phys. Rev. B **38** 11337 (1994).
- [6] Radaelli, P.G., Jorgensen, J.D., Kleb, R., Hunter, B.A., Chou, F.C., Johnston, D.C., Phys. Rev. B **49**, 6239 (1994).
- [7] Grande. B. Von, Müller-Buschbaum, Hk., and Schweizer, M., Z. Anorg. Allg. Chem. **428**, 120 (1977).
- [8] Birgeneau, R.J., and Shirane, G., in *Physical Properties of High Temperature Superconductors I*, ed. Ginsberg, D.M. (World Scientific, 1989) pp. 151-212 and references therein.
- [9] Radaelli, P.G., Jorgensen, J.D., Schultz, A.J., Hunter, B.A., Wagner, J.L., Chou, F.C., and Johnston, D.C., Phys. Rev. B **48**, 499 (1993).
- [10] Vaknin, D., Zaretsky, J.L., Johnston, D.C., Schirber, J.E., and Fisk, Z., Phys. Rev. B **49**, 9057 (1994).
- [11] Takayama-Muromachi, E., Sasaki, T., and Matsui, Y., Physica C **207** 597 (1990).
- [12] Tranquada, J.M., Buttrey, D. J., and Rice, D.E., Phys. Rev. Lett. **70**, 445 (1993); Tranquada, J.M., Kong, Y., Lorenzo, J.E., Buttrey, D.J., Rice, D.E., and Sachan, V., Phys. Rev. B **50**, 6340 (1994).

- [13] Safran, S., Sol. St. Phys. **40**, 183 (1987).
- [14] The top-seeded-solution grown crystals were grown using a technique very similar to that described in Hidaka, Y., Enomoto, Y., Suzuki, M., Oda, M. and Murakami, T., J. Crystal Growth **91**, 463 (1988).
- [15] Cheong, S.W., et al., Solid State Commun. **65**, 111 (1988).
- [16] Chou, F.C., Johnston, D.C., Cheong, S.W., and Canfield, P.C., Physica C **216**, 66 (1993).
- [17] Thio, T., Thurston, T.R., Preyer, N.W., Picone, P.J., Kastner, M.A., Jenssen, H.P., Gabbe, D.R., Chen, C.Y., Birgeneau, R.J., and Aharony, Amnon, Phys. Rev. B **38** 905 (1988); Thio, T., and Aharony, A., Phys. Rev. Lett. **73**, 894 (1994).
- [18] Birgeneau, R.J., Gabbe, D.R., Jenssen, H.P., Kastner, M.A., Picone, P.J., Thurston, T.R., Shirane, G., Endoh, Y., Sato, M., Yamada, K., Hidake, Y., Oda, M., Enomoto, Y., Suzuki, M., and Murakami, T., Phys. Rev. B **38**, 6614 (1988).
- [19] Zhou, J.S., Chen, H., and Goodenough, J.B., Phys. Rev. B **50** 4168 (1994).
- [20] Quijada, M.A., Tanner, D.B., Chou, F.C., Johnston, D.C., and Cheong, S.-W., Preprint.
- [21] Chaillout, C., Cheong, S.W., Fisk, Z., Lehmann, M.S., Marezio, M., Morosin, B., and Schirber, J.E., Physica C **158**, 183 (1989).
- [22] Zolliker, P., Cox, D.E., Parise, J.B., McCarron III, E.M., and Farneth, W.E., Phys. Rev. B **42**, 6332 (1990).
- [23] Chaillout, C., Chenavas, J., Cheong, S.W., Fisk, Z., Marezio, M., Morosin, B., and Schirber, J.E., Physica C **170**, 87 (1990).
- [24] Hammel, P.C., Reyes, A.P., Cheong, S.-W., Fisk, Z., and Schirber, J.E., Phys Rev. Lett. **71**, 440 (1993); Hammel, P.C., Statt, B.W., Chou, F.C., Johnston, D.C., Fisk, Z., Cheong, S.W., and Schirber, J.E., to be published in the proceedings of the conference “Anharmonic Properties of High TC Cuprates” held in Bled, Slovenia, Sept. 1-6, 1994.
- [25] Lorenzo, J.E., Tranquada, J. M., Buttrey, D.J., and Sachan, V., Phys. Rev. B **51**, 3176 (1995).

[26] Chou, F.C., and Johnston, D.C., Preprint

Figure Captions

Fig. 1 Magnetization as a function of temperature for an applied field of 0.5 T. There is a peak in each scan at the Néel temperature that is indicative of the weak ferromagnetic transition. The electrolysis process was stopped at regular intervals in order to take the magnetization data. The data set labeled (1) was taken on the as-grown crystal before oxidation. Data set (2) was taken after one week of electrolysis, set (3) after two weeks and set (4) after four weeks. The lines are guides to the eye.

Fig. 2 Parts a and b are a schematic structure for $\text{La}_2\text{CuO}_{4+\delta}$. An \mathbf{a} -axis projection of the real space structure is shown in (a) for the undoped $\delta=0$ phase and in (b) for the model stage 4 structure. The double triangles represent CuO_6 octahedra, and the La atoms are left out for clarity. The dashed lines indicate octahedra displaced by $\mathbf{a}/2$ out of the plane of the paper with respect to the octahedra drawn with solid lines. Figure 2c is a reciprocal-space map of the allowed reflections of the two structures for the $[\text{H},0,\text{L}]/[0,\text{K},\text{L}]$ scattering zone. The solid circles indicate the positions of the fundamental peaks present in both structures, the open triangles are the Bmab superstructure peaks for the oxygen-poor phase and the open circles are the stage 4 superlattice peaks for the oxygen-rich phase.

Fig. 3 Neutron scattering scans along the reciprocal space L direction revealing the superlattice peaks detected in various crystals. The peak at the $(0,1,4)$ position is a Bmab superlattice peak and is cut off in the lower panels to emphasize the staging peaks. The vertical dashed lines are included for reference at $(0,1,4 \pm \frac{1}{4})$. The solid curve in the bottom panel is a guide to the eye.

Fig. 4 Scan along L in the vicinity of the $(0,3,2)$ position for sample B showing superlattice peaks due to both the oxygen-poor, Bmab phase and the oxygen-rich, stage 4 phase. This wide scan shows that the oxygen-rich phase has strong peaks at $(0,3,2 \pm \frac{1}{4})$, but at best barely detectable peaks at $(0,3,2 \pm \frac{3}{4})$ with only a very weak signal at $(0,3,1\frac{1}{4})$ and no intensity above background at $(0,3,2\frac{3}{4})$.

Fig. 5 Lattice parameters as a function of temperature for several samples of $\text{La}_2\text{CuO}_{4+\delta}$. The top panel shows the \mathbf{c} lattice constant and the lower panel shows the in-plane lattice constants.

The open symbols are for the minority oxygen-poor phases and the solid symbols are for the oxygen-rich phase and cannot be independently measured.

Fig. 6 The temperature dependence of the out-of-plane half-width at half-maximum (HWHM), in-plane HWHM, and the integrated peak intensity for the $(0,3,1\frac{3}{4})$ peak for two different samples with stage 4 phases. The HWHM and intensities were determined by fits to the peaks of a 3D Lorentzian squared profile convolved with the instrumental resolution.

Fig. 7 Magnetization for sample E as a function of temperature. The top panel shows a high-field scan revealing the weak ferromagnetic transition of the oxygen-poor phase and the lower panel show zero field cooled measurements of the shielding signal of the oxygen-rich superconducting phase.

Fig. 8 Neutron scattering scans at room temperature (open circles) and 10K (filled circles) showing the effects of phase separation and stage ordering. The top panel shows the emergence of the $(0,1,4 \pm 0.15)$ staging peaks at low temperatures. The bottom panel shows the $(0,0,8)$ peak revealing a single c -axis at room temperature which is split to reveal two phases with different c -axes at low temperatures.

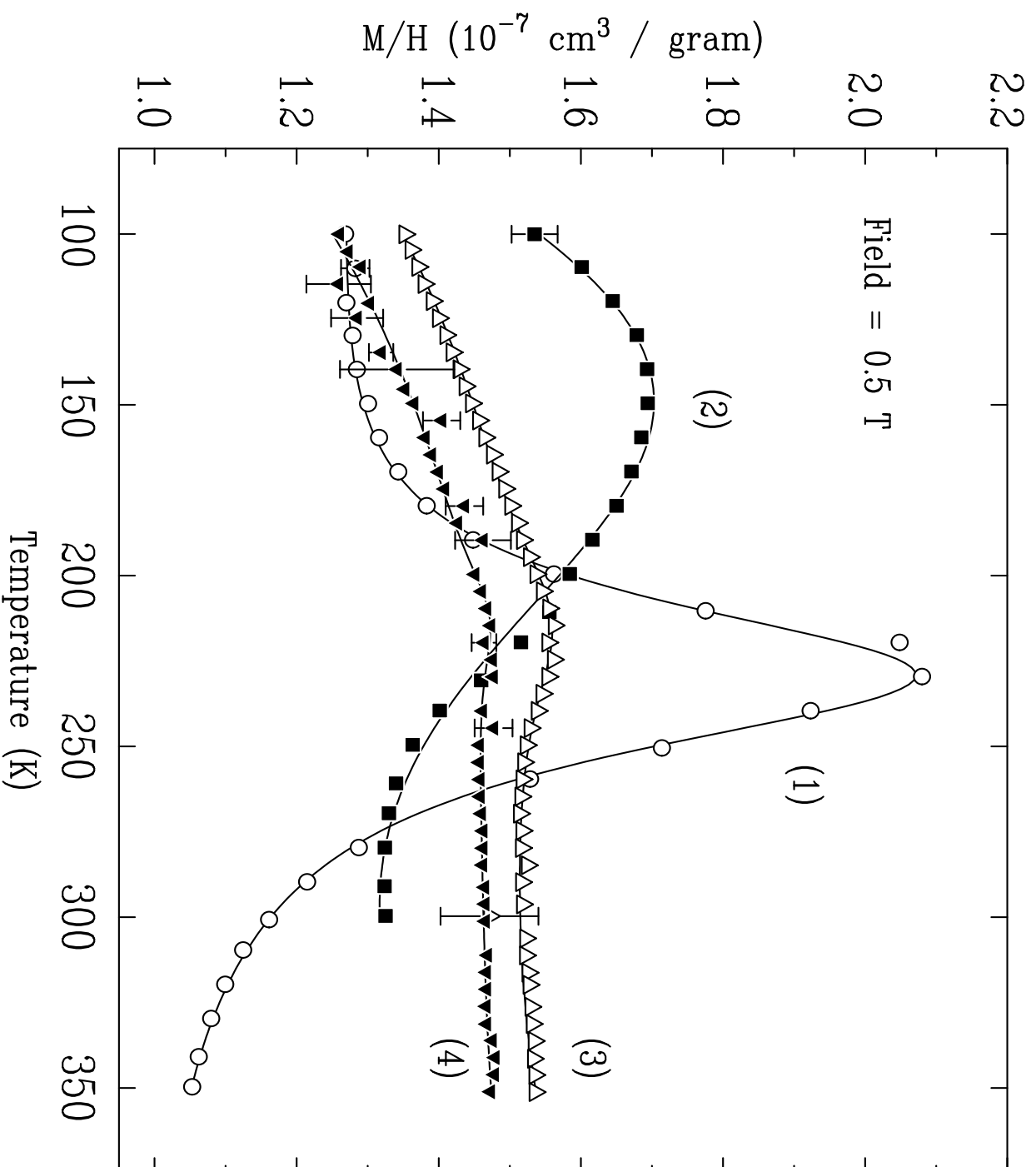


Figure 1

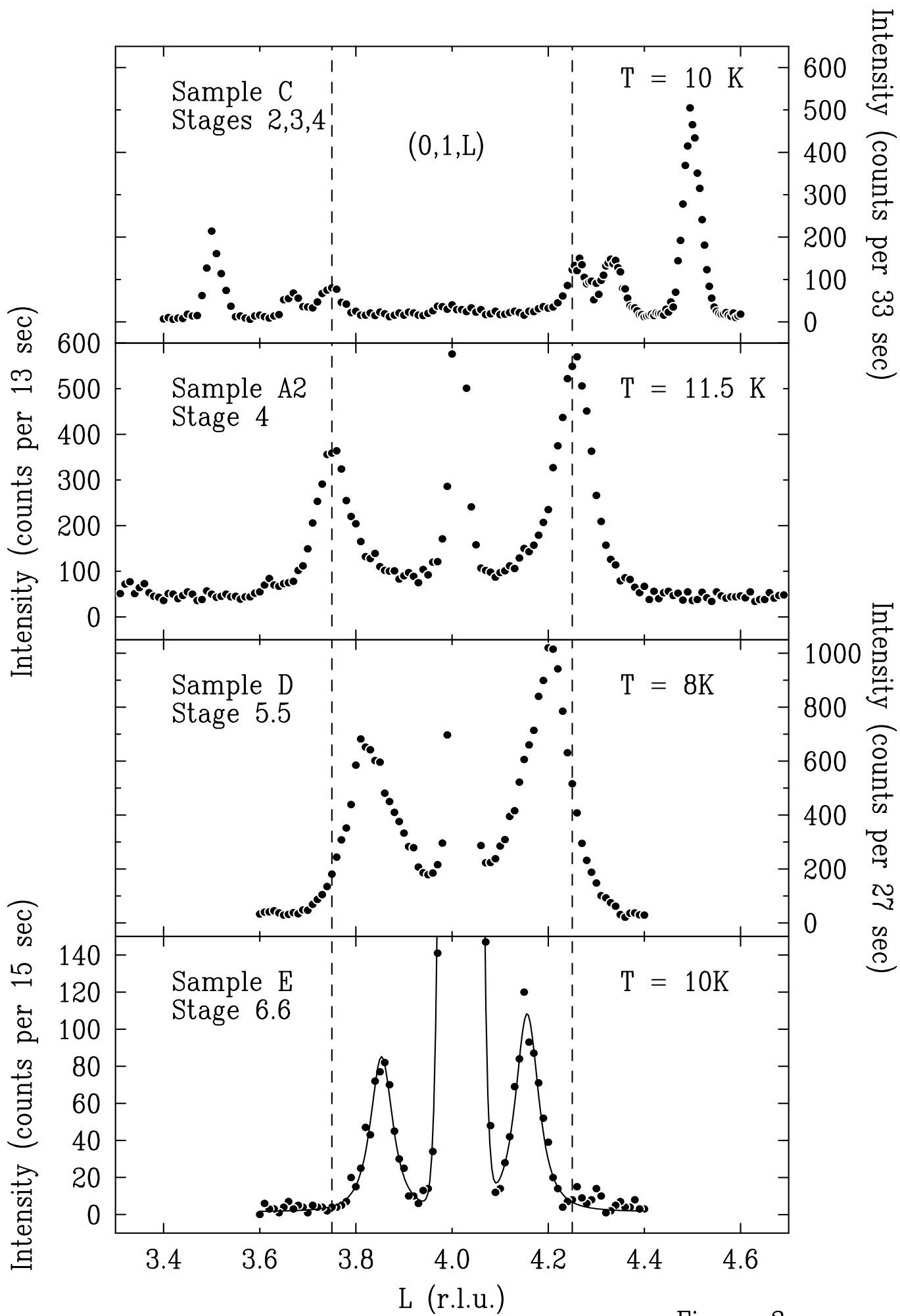


Figure 3

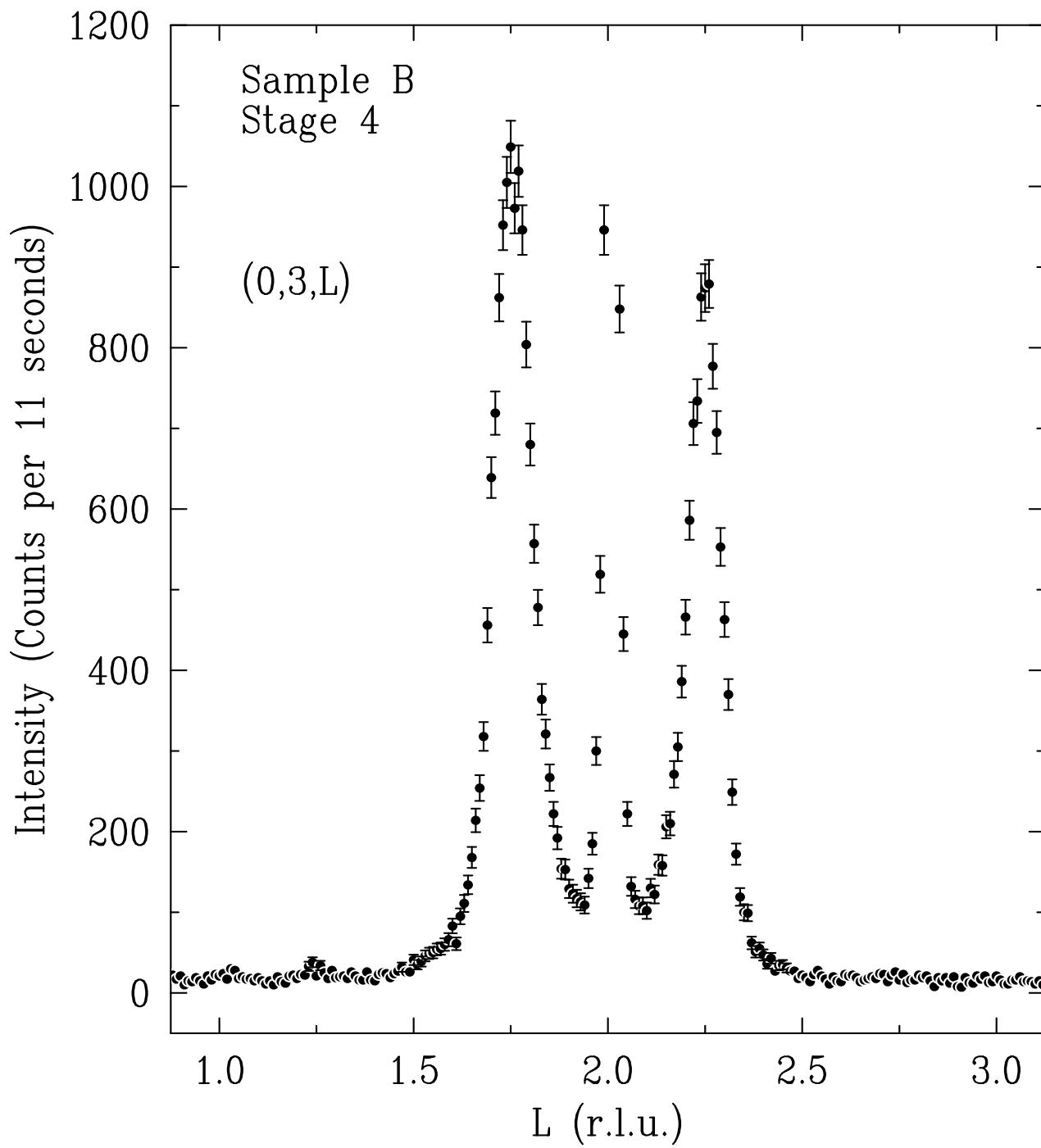


Figure 4

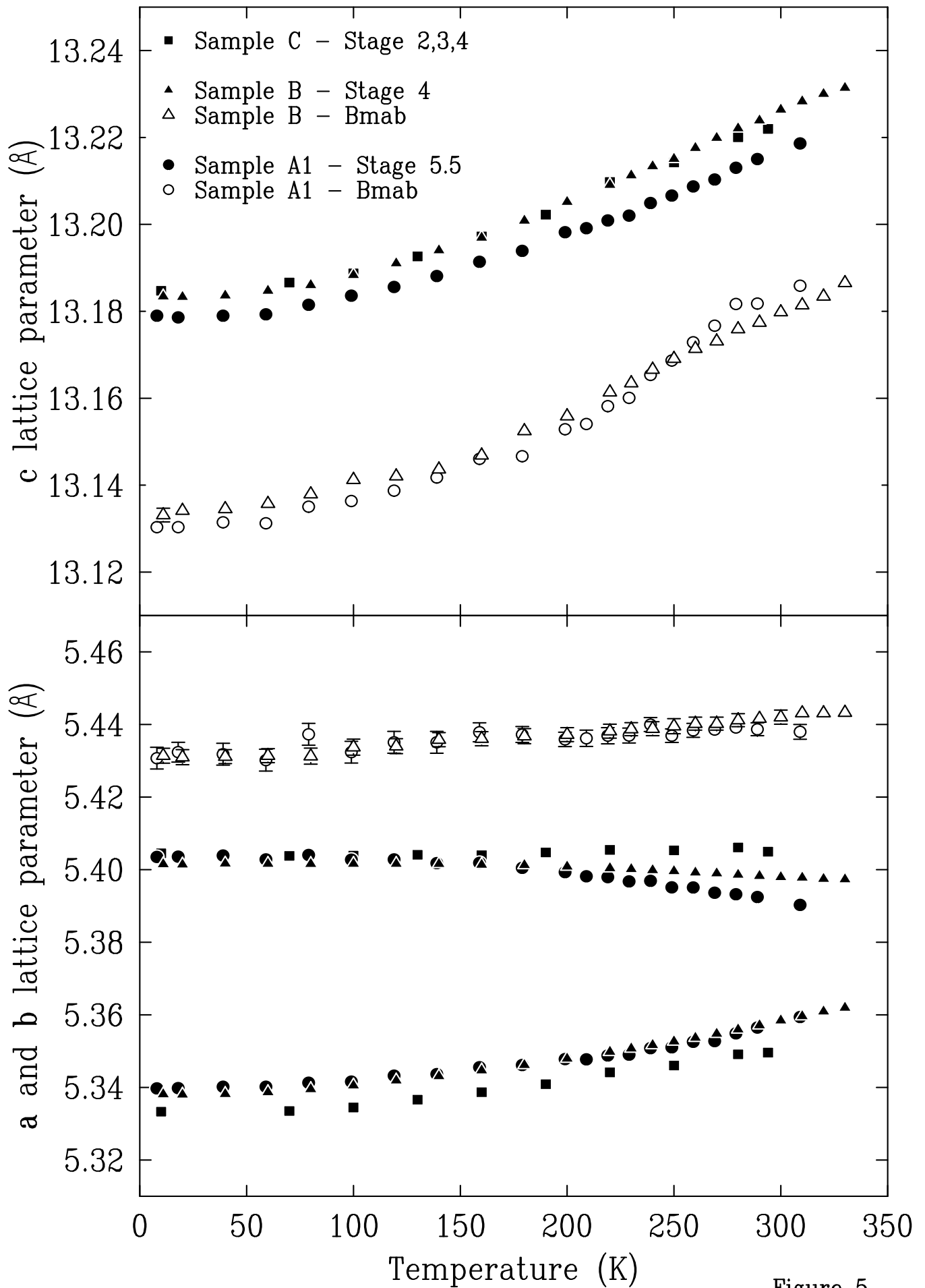


Figure 5

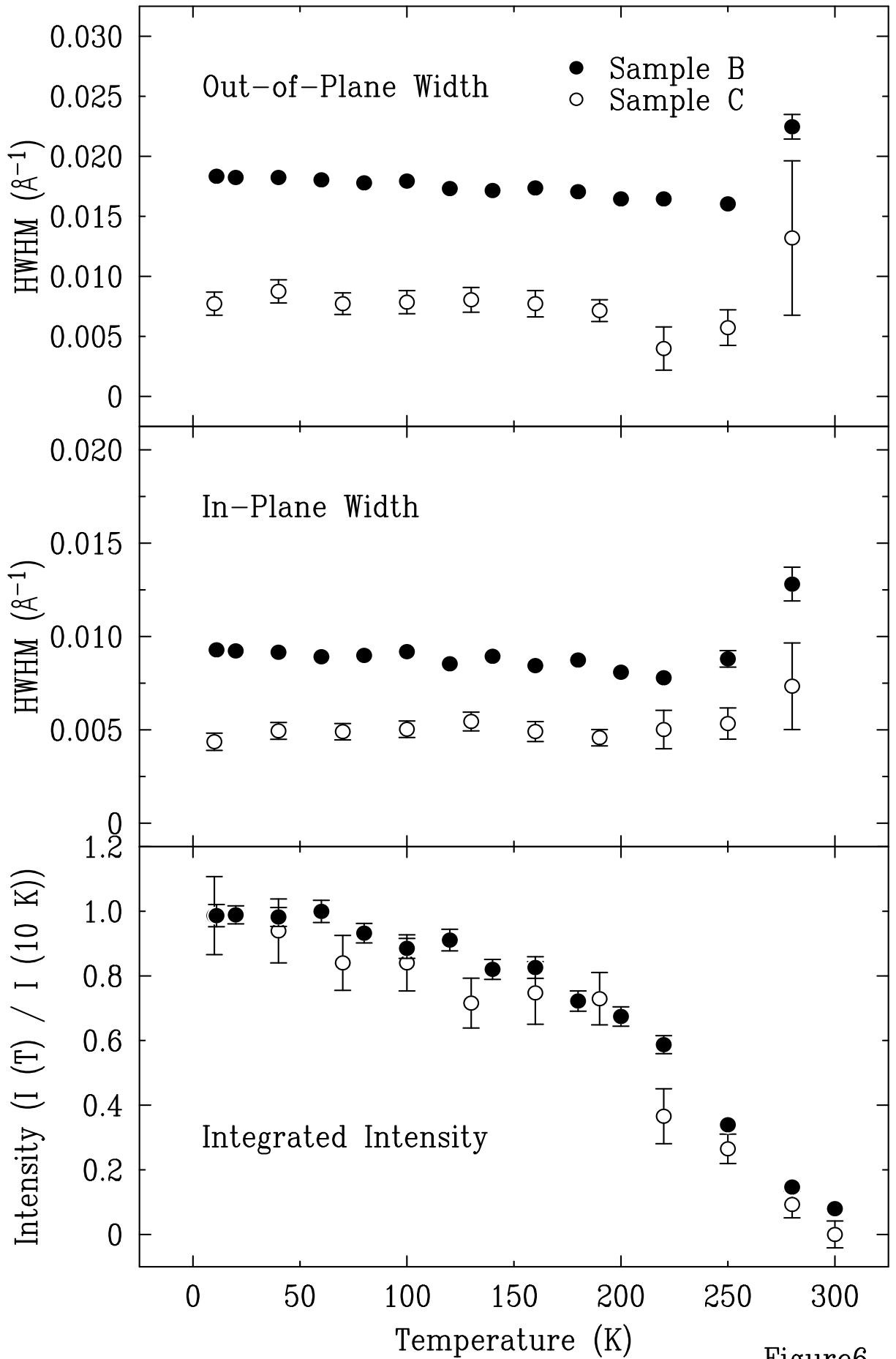


Figure6

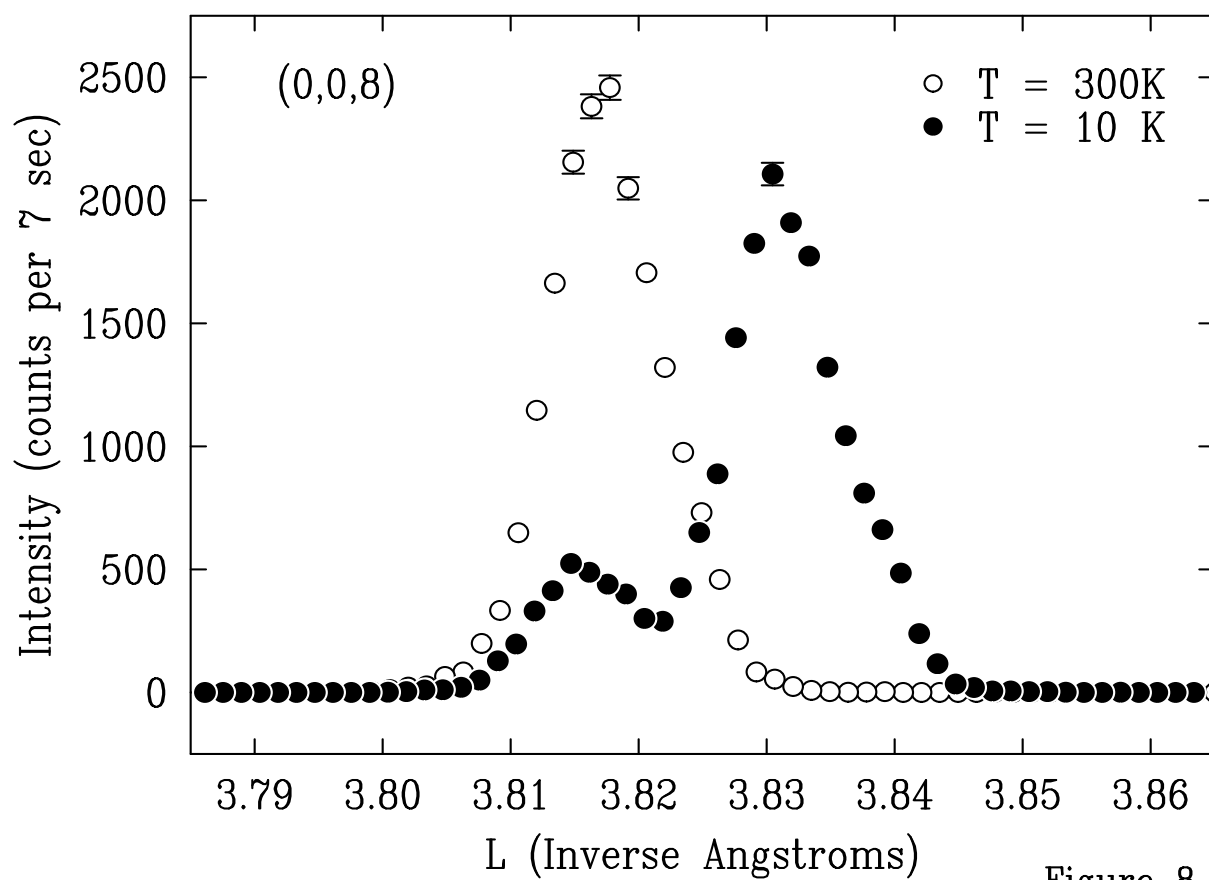
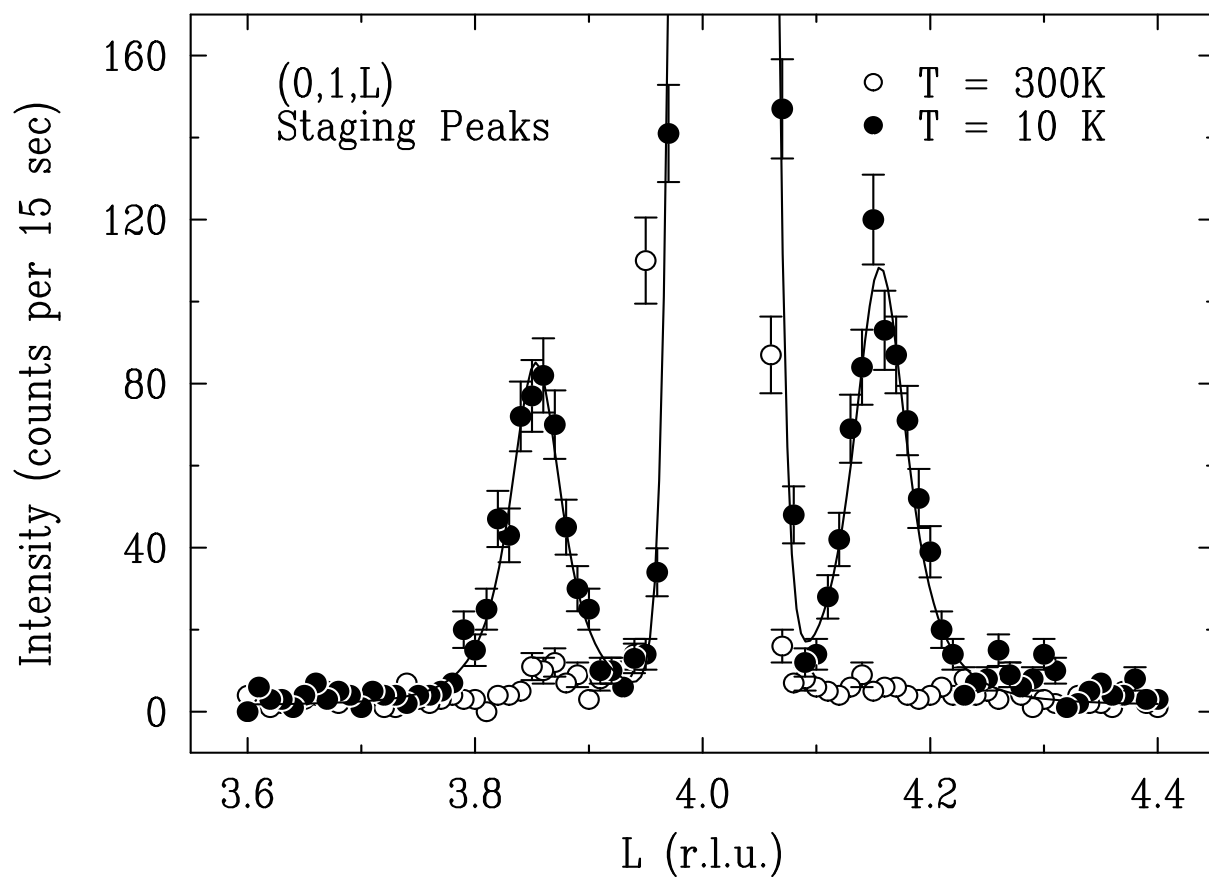


Figure 8